2020 Fifteenth International Conference on Ecological Vehicles and Renewable Energies (EVER)

Power- and Current-Based Control of Distributed Inverters in Low-Voltage Microgrids: Considerations in Relation to Classic Droop Control

Augusto M. S. Alonso, Fernando P. Marafao
Sao Paulo State University
Group of Automation and Int. Systems
Sorocaba 18087-180, Brazil
Email: augusto.alonso@unesp.br; fernando.marafao@unesp.br

Augusto M. S. Alonso, Fredrik Göthner, Elisabetta Tedeschi
Norwegian University of Science & Technology
Department of Electric Power Engineering
Trondheim 7034, Norway
Email: fredrik.gothner@ntnu.no; elisabetta.tedeschi@ntnu.no

Danilo I. Brandao
Federal University of Minas Gerais
Graduate Program in Electrical Engineering
Belo Horizonte 31270-901, Brazil
Email: dibrandao@ufmg.br

***Abstract*—This paper addresses the matter of active and reactive power sharing among distributed inverters in low-voltage microgrids, particularly highlighting the peculiarities of two strategies of coordinated control based on a master/slave architecture, namely Power- and Current-Based Control, in comparison to the classic droop control approach. It is demonstrated that the Power- and Current-Based Control strategies present distinct operational features in relation to classic droop control, mostly concerning how active and reactive power are shared among inverters. Additionally, it is shown how the strategies differ in steady-state operation and response time while comparing to classic droop-based methods. Discussions are presented based on simulation results using Matlab/Simulink, comprising two distributed inverters in a low-voltage microgrid and considering different operational scenarios, such as load changes, existence of linear and nonlinear loads, as well as line impedance variations. Experimental results are presented to validate the expected behavior of one of the strategies.**

Keywords*—*Current-Based Control, droop control, microgrids, Power-Based Control, power sharing

I. INTRODUCTION

The intensified penetration of renewable sources and distributed generation in low-voltage (LV) networks is imposing a new power electronics-based perspective to the electrical scenario [1], [2]. As power electronic interfaces (PEIs) spread over such electrical networks, the challenges related to their cooperative operation, such as proper power sharing among inverters existing within distributed generators (DGs), have become of significant importance to bring to reality the perspective of smart microgrids (MGs) [3], [4]. As a matter of fact, it has been demonstrated that without adequate cooperation among PEIs, MGs are prone to instable operation [5], to not comply with power quality standards and codes [6], and likely to be economically non-attractive [7].

Coordination of PEIs in MGs have been proposed in literature basically following centralized, decentralized or distributed approaches [8], which are even being mixed to evolve to more a digitized paradigm, as for instance, the incorporation of concepts such as the internet of things (IoT) [9], as seen in Fig. 1. Centralized strategies for coordination of inverters in MGs mainly require a master/central controller (CC) unit, on which the electrical quantities (e.g., currents, voltages, power terms) and other control data (e.g., scaling coefficients, etc.) are processed. Therefore, in a master/slave strategy, data is required to be exchanged from/to the CC with each participating unit (i.e., distributed inverters) [8], [10]. The master unit holds the server, while the slave units are clients. Thus, communication links play an important role on the cooperative operation of the inverters [11].

On the other hand, decentralized coordination of PEIs, in general, does not rely on any data exchange among the participating units for inaccurately sharing the power among DGs, which overcomes issues inherited by limitations in communication channels existing in centralized approaches [4]. At most, low-bandwidth communication links might be used in decentralized strategies as means for correcting inconsistencies in layered control loops (i.e., such as in hierarchical control methods [4,6,11]). Despite that, although issues related to communication is majorly absent, other issues such as poor power sharing accuracy may occur [12], [13]. Distributed control, by its turn, merges the centralized and decentralized methods by using communication to share the required control data among many participating units, not relying on a CC [12].

In literature [4]-[12], droop control is by far the most adopted strategy to coordinate inverters, especially for decentralized and distributed methods. This occurs since

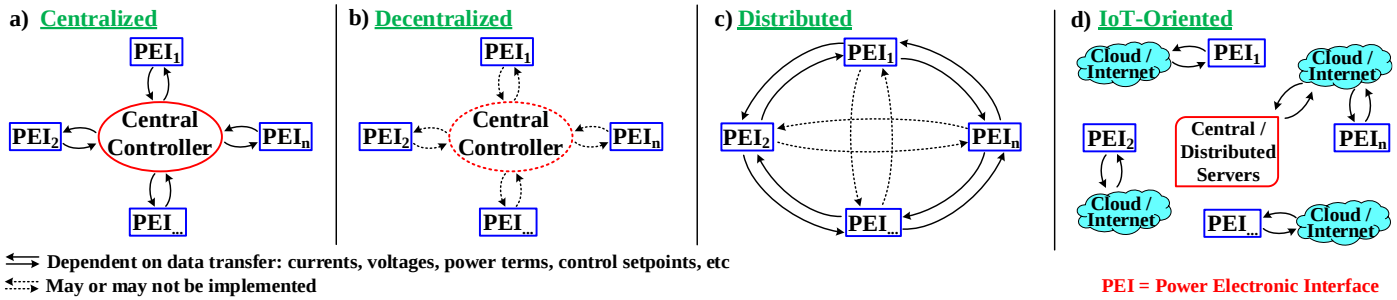

Fig. 1: Control topologies for cooperative operation of distributed inverters in microgrids.

droop-based approaches generally steer inverters under voltage-controlled mode (VCM) [4], which basically requires only local electrical quantities (e.g., voltages, currents, power terms) to be processed by the parallel inverters, while the cooperative operation itself is achieved as result of the tuning of droop gains [4], [14]. Due to its simplicity, droop control is easily implemented; however, many variations on this classic method have been recently proposed [12,15,16] to overcome inherited issues of inaccurate power sharing, dependence on the knowledge of physical parameters, and sensitivity related to variations within MG's (e.g., dynamic impedance changes on the circuit).

Knowing that centralized, decentralized and distributed control strategies present particular advantages and disadvantages, aiming at extending the capability to exploit PEIs, two master/slave-based approaches were proposed, being formulated by the analysis of power [10] and current [17] terms flowing within a MG. Firstly, the so-called Power-Based Control (PBC) method, was proposed in [10] aiming at achieving full controllability of PEIs operating under current-controlled mode (CCM). Consequently, the offering of active and reactive power sharing could be achieved under an accurate means and without requiring previous information from the MG physical system. It is reinforced that the power-based formulation of [10] that is herein considered is different from [18], since the latter is based on the analysis and transmission of complex power quantities.

The PBC strategy, as in [10], then evolved by extending its capability to also provide coordination of PEIs striving for unbalance compensation [19], to accommodate both VCM and CCM operation of PEIs [20], to control single- and three-phase topologies [21], and others [22]. Moreover, taking advantage of the same MG infrastructure and operational features, although relying on a significantly different formulation in relation to the PBC, the Current-Based Control (CBC) was proposed in [17]. The main concept behind the CBC method is the analysis of peak currents flowing through the MG, instead of power terms as in the PBC, not only to provide active and reactive power sharing among inverters, but also to achieve distributed harmonic compensation, as well as voltage resonance damping [23].

Despite the fact that many works have being exploring and demonstrating the capabilities of both PBC and CBC methods, to the best of the author's knowledge, no study found in literature provides discussions in relation to how such approaches operate in relation to the well-known droop control. Thus, the main contribution of this paper is settled. Herein, the goal is to describe the operation of the PBC and CBC strategies, as well as the classic droop control method, demonstrating how they perform in coordinating parallel inverters. Focus is given to the sharing of active and reactive power, and a single-phase circuit topology is considered for the sake of simplicity.

This paper is structured as follows. In Section II, the adopted MG topology and the PBC and CBC strategies are explained, being followed by a brief presentation of the classic droop control method in Section III. Simulation results are presented in Section IV as groundwork for the discussions related to operational peculiarities of the PBC and CBC methods in relation to classic droop control. In Section V experimental results of the CBC strategy are presented to reiterate the discussions in regard to how such master/slave methods perform. Conclusions seen in Section VI highlight the main considerations presented within this paper, and proposals for extension of discussions are raised for future works.

II. Power- and Current-Based Control Strategies

Aiming at steering PEIs in LV MGs with accuracy and under a coordinated approach, the PBC and CBC were conceived based on centralized methodologies that relies on the same control infrastructure, comprising of a MG that can connect or disconnect from a main grid as seen in Fig. 2. Since these methods were proposed primarily focusing on the offering of power sharing among inverters interfacing dispatchable power generations (e.g., as PV and wind-based generation system), PEIs are herein considered to operate as ideal current sources (i.e., operating under CCM).

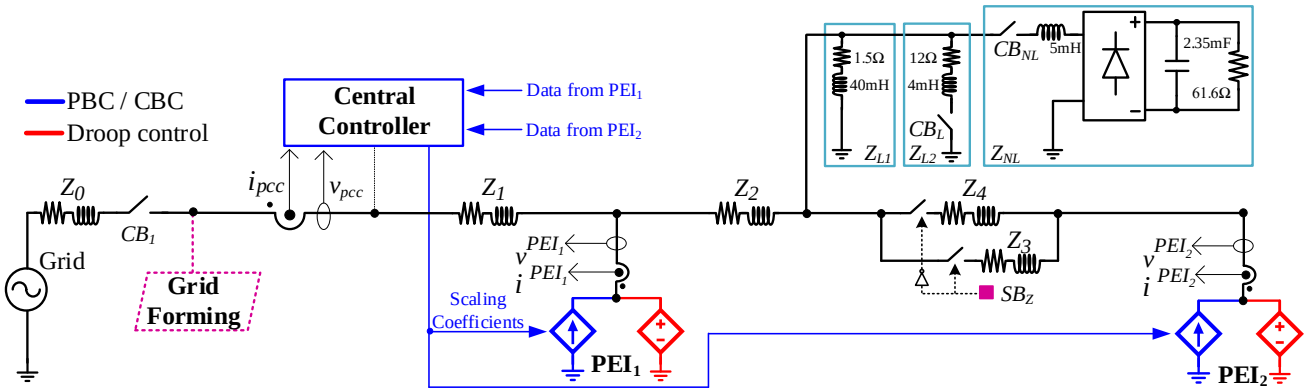

Fig. 2: Circuit setup adopted for discussions related to the MG topology and control strategies, as well as implemented for simulation and experimental results.

Consequently, different from droop control that steers PEIs under VCM, for both the PBC and CBC strategies, a grid-forming converter [14] is required to be placed at the point-of-common-coupling (PCC) of the MG to provide islanded operation. Moreover, although both PBC and CBC are able to accommodate VCM inverters on their methodology by adjusting local power/current control loops [24], for the sake of simplicity, this is not considered herein.

The master/slave approach considered requires the existence of a CC, which is responsible to process the PBC or CBC algorithms (i.e., based on electrical quantities flowing through the PCC), and also using information about powers [10] or peak currents [17] flowing at the branch of each participating PEI. Thus, for both methods, the CC plays the role of a master unit, while inverters are steered as slave units, adjusting their power or current injection according to scaling coefficients broadcasted by the CC through the communication link. A brief explanation regarding the calculations required for the PBC and CBC is presented in the following.

A. *Power-Based Control Strategy*

To achieve power sharing in a single-phase MG by means of the PBC, the active and reactive power flowing at the PCC, as well as the one being processed by each PEI, are required to be calculated [10]. As aforementioned, the local active (P_{PEI_j}) and reactive (Q_{PEI_j}) power of each *j*-th PEI are periodically sent to the CC, along with the information of their active power capability and nominal apparent power, respectively, $P_{PEI_j}^{max}$ and S_{PEI_j}. Since the CC is placed at the PCC, as in Fig. 2, it also measures the active (P_{Grid}) and reactive (Q_{Grid}) power at this point.

Thus, at a given control cycle *k*, the CC computes the total (i.e., superscript "*t*") active and reactive power processed by the PEIs through (1) and (2), and the total capacity of the MG for active power generation (3). In addition, the maximum contribution of reactive power from all PEIs is given by (4), where S_{PEI}^{t} is the total nominal power considering the *J* inverters being coordinated.

$$P_{PEI}^{t}(k) = \sum_{j=1}^{J} P_{PEI_j}(k) \tag{1}$$

$$Q_{PEI}^{t}(k) = \sum_{j=1}^{J} Q_{PEI_j}(k) \tag{2}$$

$$P_{PEI}^{max\ t}(k) = \sum_{j=1}^{J} P_{PEI_j}^{max}(k) \tag{3}$$

$$Q_{PEI}^{max\ t}(k) = \sqrt{[S_{PEI}^{t}(k)]^2 - \left[P_{PEI}^{max\ t}(k)\right]^2} \tag{4}$$

The power balance of the active and reactive terms being processed at the MG leads to (5) and (6), on which P_{Grid} and Q_{Grid} are the active and reactive components measured at the PCC; and P_L and Q_L are the powers drawn by the loads.

$$P_L(k) = P_{Grid}(k) + P_{PEI}^{t}(k) \tag{5}$$

$$Q_L(k) = Q_{Grid}(k) + Q_{PEI}^{t}(k) \tag{6}$$

By knowing the load power, the power references for the next control cycle $k+1$, $P_{PEI}^{t*}(k+1)$ and $Q_{PEI}^{t*}(k+1)$, can be calculated by (7) and (8), considering that $P_{Grid}^{*}(k+1)$ and $Q_{Grid}^{*}(k+1)$ are the desired powers to flow through the PCC.

$$P_{PEI}^{t*}(k+1) = P_L(k) - P_{Grid}^{*}(k+1) \tag{7}$$

$$Q_{PEI}^{t*}(k+1) = Q_L(k) - Q_{Grid}^{*}(k+1) \tag{8}$$

Finally, the scaling coefficients that steer the PEIs to offer active (α_P) and reactive (α_Q) power sharing proportionally to their capacities are given by (9) and (10). Such coefficients are in the range [-1, 1] and relate to injection/absorption of active power and injection of inductive/capacitive reactive power.

$$\alpha_P = \frac{P_{PEI}^{t*}(k+1)}{P_{PEI}^{max\ t}} \tag{9}$$

$$\alpha_Q = \frac{Q_{PEI}^{t*}(k+1)}{Q_{PEI}^{max\,t}} \tag{10}$$

Therefore, each PEI can adjust its injection of active and reactive power by using the references given by (11) and (12) on their local controllers.

$$P_{PEI_j}(k+1) = \alpha_P * P_{PEI_j}^{max} \tag{11}$$

$$Q_{PEI_j}(k+1) = \alpha_Q * Q_{PEI_j}^{max} \tag{12}$$

B. *Current-Based Control Strategy*

Following the same operational approach as the PBC method, the CBC strategy is formulated in single-phase systems by analyzing peak currents processed by the PEIs, as well as the ones flowing through the PCC [17]. Each inverter *j* needs to measure its output time-domain current (i^{PEIj}) and voltage (v^{PEIj}), using the latter to detect the synchronization angle (θ). Afterwards, by feeding θ to sine and cosine functions, unitary in-phase and quadrature signals, $x_{h\parallel}$ and $x_{h\perp}$, can be used onto a discrete Fourier transform (DFT) method to decompose i^{PEI} and attain its in-phase and quadrature peak values, $I_{h\parallel}^{PEIj}$ and $I_{h\perp}^{PEIj}$, for each harmonic *h* of interest to be controlled. In [17] a thorough explanation is presented concerning how such local decomposition is performed for the calculation of the peak currents. Since in this paper focus is given to active and reactive power sharing only, *h = 1*, and the processing of other harmonics than the fundamental is disregarded. Thus, each PEI sends its processed fundamental active ($I_{1\parallel}^{PEIj}$) and reactive ($I_{1\perp}^{PEIj}$) peak currents to the CC at the given control cycle *k*, along with its nominal peak current capability (I_{nom}^{PEIj}), as well as the maximum active current able to be generated at that given instant (I_{max}^{PEIj}).

Following the same procedure done by the PEIs, the CC measures the local time-domain voltage, v^{pcc}, to attain the PCC's synchronization angle that is later used to decompose the current i^{pcc} being drawn from the main grid, or from the grid-forming converter if the MG operates under islanded mode. Now, by gathering the data packets from all participating units, similarly to the approach of the PBC strategy, the CBC approach requires the CC to compute the total active ($I_{1\parallel}^{PEIt}$) and reactive ($I_{1\perp}^{PEIt}$) peak current injection provided by the PEIs, as given by (13) and (14). Likewise, (15) and (16) calculate the overall capability of the MG for active power generation and the nominal limits.

$$I_{1\parallel}^{PEIt}(k) = \sum_{j=1}^{J} I_{1\parallel}^{PEIj}(k) \tag{13}$$

$$I_{1\perp}^{PEIt}(k) = \sum_{j=1}^{J} I_{1\perp}^{PEIj}(k) \tag{14}$$

$$I_{max}^{PEIt}(k) = \sum_{j=1}^{J} I_{max}^{PEIj}(k) \tag{15}$$

$$I_{nom}^{PEIt}(k) = \sum_{j=1}^{J} I_{nom}^{PEIj}(k) \tag{16}$$

Similarly to (5) and (6), but using Kirchhoff's current law, one can attain the load currents drawn at the MG from (17) and (18), leading to (19) and (20), the active and reactive peak current references for the MG, which shall be used as reference for current sharing among PEIs.

$$I_{1\parallel}^{L}(k) = I_{1\parallel}^{Grid}(k) + I_{1\parallel}^{PEIt}(k) \tag{17}$$

$$I_{1\perp}^{L}(k) = I_{1\perp}^{Grid}(k) + I_{1\perp}^{PEIt}(k) \tag{18}$$

$$I_{1\parallel}^{*}(k+1) = I_{1\parallel}^{L}(k) - I_{1\parallel}^{Grid\,*}(k+1) \tag{19}$$

$$I_{1\perp}^{*}(k+1) = I_{1\perp}^{L}(k) - I_{1\perp}^{Grid\,*}(k+1) \tag{20}$$

Finally, scaling coefficients, $\alpha_{1\perp}$ and $\alpha_{1\parallel}$, can be calculated for, respectively, the active and reactive current balancing at all PEIs following (21) and (22). The peak current capability of the network, $\sqrt{\Delta I}$, is calculated sequentially, firstly for the active current injection, and then having $\Delta I = (I_{nom}^{PEIt})^2 - (I_{1\parallel}^{PEIt})^2$), which is used for the reactive current, similar to what is done for the active and reactive power in (9) and (10). Yet, having that $I_{1\parallel}^{PEIt}$ is limited to I_{max}^{PEIt}.

The final time-domain reference (i^{j*}) to be used on the current controllers of each inverter *j* is then obtained from (23), where $\sqrt{\Delta I^j}$ is the local current capability of the PEI, which is calculated sequentially for the active and reactive current injections as done for $\sqrt{\Delta I}$.

$$\alpha_{1\parallel} = \frac{I_{1\parallel}^{*}(k+1)}{\sqrt{\Delta I}} \tag{21}$$

$$\alpha_{1\perp} = \frac{I_{1\perp}^{*}(k+1)}{\sqrt{\Delta I}} \tag{22}$$

$$i^{j*} = \underbrace{\left(\alpha_{1\parallel} \cdot \sqrt{\Delta I^j}\right)}_{I_{1\parallel}^{j*}} \cdot x_{1\parallel}^{j} + \underbrace{\left(\alpha_{1\perp} \cdot \sqrt{\Delta I^j}\right)}_{I_{1\perp}^{j*}} \cdot x_{1\perp}^{j} \tag{23}$$

As can be seen from its formulation, the CBC presents a harmonic-dependent feature, which may be further explored to provide distributed harmonic current compensation along with the fundamental active and reactive current sharing. Nonetheless, to provide more consistency in comparing the CBC to droop methods while providing harmonic sharing, such feature should be contrasted to decentralized strategies such as the use of virtual impedance methods [16], turning out to be out

of scope in this paper. Thus, harmonic sharing is not further discussed in this paper. Additionally, since the analysis of PCC quantities is an inherent part of the CBC and PBC strategies, one interesting operational feature of both methods is the capability to provide dispatchable power flow control at the MG's PCC, which is not straightforwardly provided by droop-based methods. Nonetheless, due to the need of extensive discussions, such matter is not addressed herein.

III. Droop Control Strategy

The conventional droop control strategy relies on a hierarchical control structure of each PEI. The inner control loops of each PEI are controlling the inverters in VCM, typically by employing cascaded voltage and current control loops. The voltage reference is provided by the droop control, which is mathematically formulated as follows for inverter *j*:

$$\omega_j = \omega_0 - m_j (P_j - P_j^*) \quad (24)$$

$$E_j = E_0 - n_j (Q_j - Q_j^*) \quad (25)$$

where ω_j and E_j are the angular frequency and voltage magnitude provided for the inner loops of inverter j, ω_0 and E_0 are the nominal values for the angular frequency and voltage of the microgrid, m_j and n_j are the active and reactive power droop gains, while P_j^* and Q_j^* are the active and reactive power references for the inverter. The terms P_j and Q_j are low-pass filtered active and reactive power supplied by the inverter. The angular frequency ω_j is integrated to get the phase angle θ_j of the inverter, as given below by (26):

$$\theta_j = \int \omega_j \, dt \quad (26)$$

IV. MG Setup and Simulation Results

In this section, simulation results are presented to demonstrate the peculiarities of the PBC and CBC strategies in relation to classic droop control. The simulated circuit is implemented in MATLAB/Simulink as shown in Fig. 2, comprising two distributed inverters in a single-phase MG that considers line impedances among nodes. The MG is set up considering nominal grid voltage of 127 V_{rms} at 60 Hz, with pure sinusoidal waveform, as well as with inverters presenting nominal apparent powers equal to $A_{PEI_1} = 5\,kVA$ and $A_{PEI_2} = 3\,kVA$. The line impedance are $Z_0 = Z_1 = Z_2 = 0.038 + j0.005$, $Z_3 = 2xZ_0$, and $Z_4 = 2xZ_3$. Two linear loads, Z_{L1} and Z_{L2}, and another nonlinear load, Z_{NL}, are implemented, as well as circuit breakers that allow the MG to be disconnected from the main grid, and to switch loads and line impedances as seen in Fig. 2.

As shown in Fig. 2, the PBC and CBC consider inverters modeled primarily as current sources, since the control architecture relies on a grid-forming converter placed at the PCC to provide MG islanded operation. Contrariwise, classic droop control considers inverters to operate as voltage sources, allowing them to impose the voltage and frequency for the MG, while also sharing the load currents. Therefore, both inverters are modeled as ideal current sources for the PBC and CBC strategies, and as ideal voltage sources for droop control. The droop gains used for the simulations are $m_{PEI_1} = 2.5e^{-5}$, $m_{PEI_2} = 4.16e^{-5}$, $n_{PEI_1} = 5e^{-5}$, $n_{PEI_2} = 8.3e^{-5}$. These were set according to the ratings of the PEIs to ensure sharing between the units. The single-phase power calculation is implemented as in [25], with a time constant of 0.03 s used for the low-pass filtering. For the PBC and CBC, the data exchange among PEIs is set to occur at rate of one cycle of a fundamental cycle (i.e., 16.66 ms). The time-controlled switch button SB_Z in Fig. 2 considers Z_3 switched on for the first scenario, and Z_4 is switched on only to provide a line impedance variation on the second study case.

Simulation results are then comprised of two scenarios. Firstly, in Figs. 3 and 4 the transient and steady state behavior of the active and reactive power for the droop-based, PBC and CBC methods are presented, as well as showing the PEIs' currents, being split into three intervals with different load conditions. Secondly, in Fig. 5, another result is presented demonstrating the behavior of the active and reactive power sharing capabilities of the methods when a line impedance variation occurs in the MG.

A. Active and Reactive Power Sharing Upon Different Load Conditions

Concerning the first scenario, which is presented in Fig. 3, Interval I considers CB_{NL} switched on and CB_L switched off, resulting in having the linear load, Z_{L1}, and the nonlinear load connected to the circuit. Thus, the loads draw active, reactive, and harmonic power. It can be seen in Interval I of Fig. 3 that, for all three methods, the active power shared by the PEIs are similar in steady state, with the droop method imposing PEI_1 to provide slightly higher active power (i.e., of about 46 W) than the PBC and CBC, as shown in Table I. Such small mismatch for the active power of the PEIs occurs since the droop method inherently has to provide the sharing of the harmonic currents being drawn by the loads. Note in Fig. 4(a) that the PBC and CBC methods are processing pure fundamental currents. Moreover, note in Table I that, since the ratio among the PEIs nominal power is $r_{PEIs} = 5/3 = 1.66$, as expected, for all the three methods, the active power is shared proportionally to the capabilities of the inverters (i.e., such ratio is maintained for the active power sharing during Interval I for all methods). Nonetheless, one of the main differences among droop control in relation to the PBC and CBC

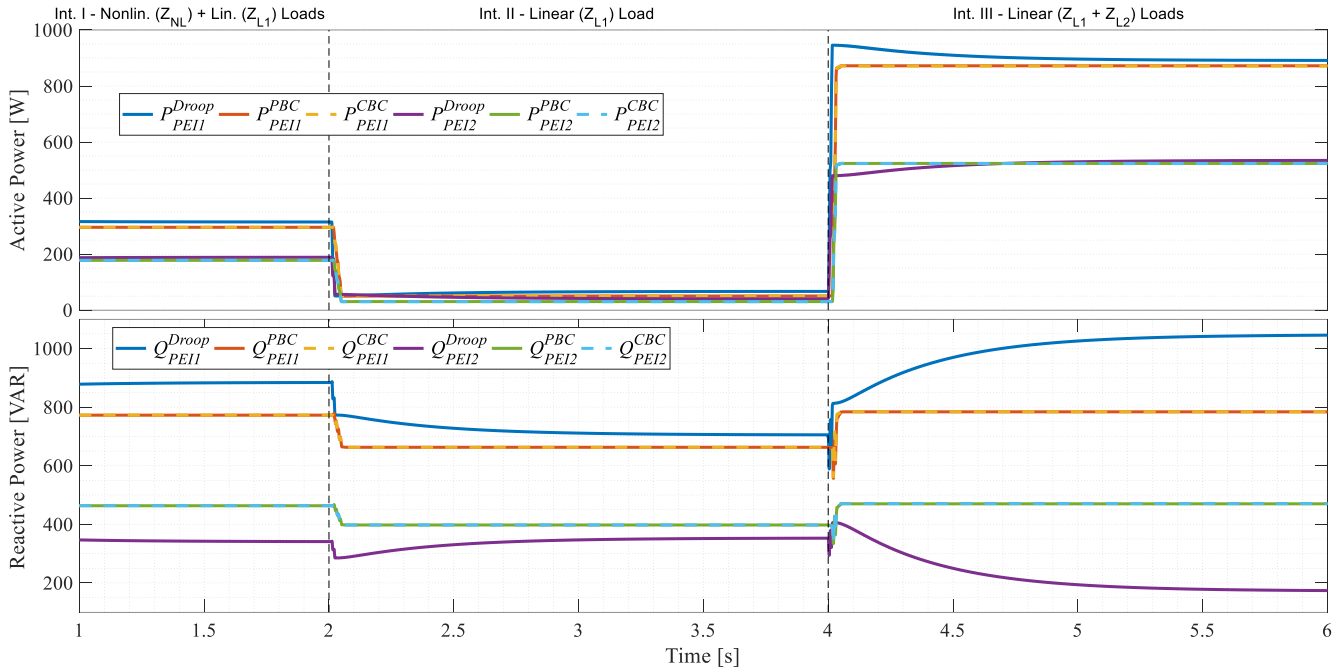

Fig. 3: Simulation results for the droop, PBC and CBC strategies sharing active and reactive power upon different load conditions.

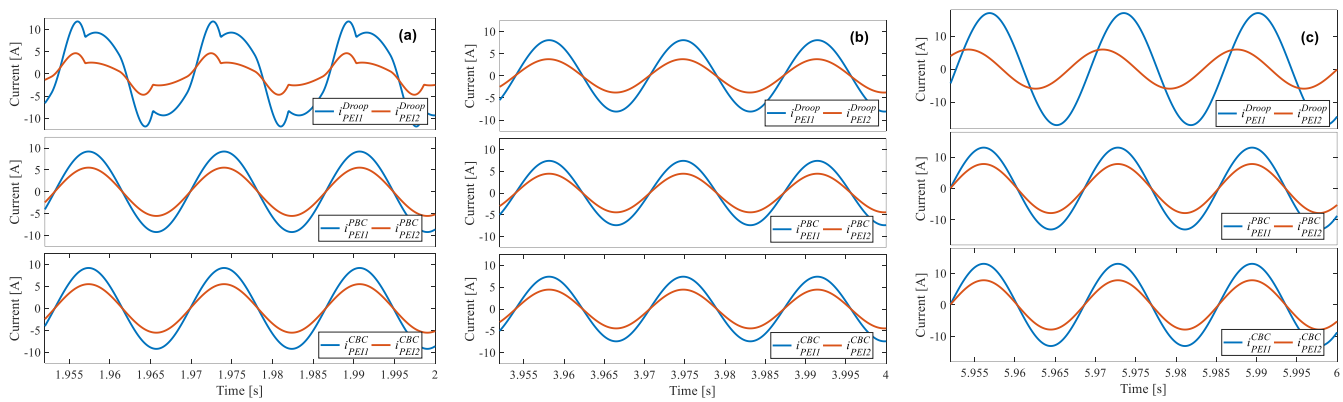

Fig. 4: Current waveforms of the inverters in (a) Interval I, (b) Interval II, and (c) Interval III for the droop (top), PBC (middle) and CBC (bottom) strategies.

TABLE 1: ACTIVE [W] AND REACTIVE [VAR] POWERS FOR RESULTS IN FIG. 3.

Method		Interval I		Interval II		Interval III	
		Active Power	*React. Power*	*Active Power*	*React. Power*	*Active Power*	*React. Power*
Droop	PEI_1	314.7	883.9	66.78	705.5	891.3	1045.1
	PEI_2	188.6	341.1	40.28	352.5	534.4	174.3
PBC	PEI_1	295.4	772.6	50.29	662.9	871.7	784.4
	PEI_2	177.3	463.6	30.17	397.7	523.2	470.8
CBC	PEI_1	295.4	772.6	50.29	662.9	871.7	784.4
	PEI_2	177.3	463.6	30.17	397.7	523.2	470.8

methods can be seen on the reactive power shared during Interval I in Fig. 3 and Table I.

Note that, different from the active power, the inverters do not share the reactive power proportionally between them for the droop method. For this case, the droop-based approach presented $r_{PEIs} = 2.59$, while the PBC and CBC maintained the proportionality ratio of $r_{PEIs} = 1.66$. This occurs due to the formulation of the classic droop method and the fact that the line impedance Z_3 is twice the value of Z_2, which leads PEIs to follow their droop equations, being sensitive to circuit parameters. The main consequence of this feature is related to the fact that, for droop control, one inverter (in this case PEI_1) had to operate offering an approximately 14 % higher apparent power than that for the PBC or CBC methods. For instance, the apparent power for PEI_1 is $A_{PEI_1}^{Droop} = \sqrt{314.7^2 + 883.9^2} = 938.25\,VA$, while for the PBC and CBC it resulted in $A_{PEI_1}^{PBC} = A_{PEI_1}^{CBC} = 827.14\,VA$. As a consequence, the opposite condition occurs to PEI_2, having the droop method resulting in $A_{PEI_2}^{Droop} = 389.76\,VA$, which is about 27 % lower than that for the other methods.

During Interval II in Fig. 3, CB_{NL} is switched off at 2.0 s, allowing only Z_{L1} to be connected to the MG, consequently reducing the amount of active and reactive power drawn by the load. Note that, the transient response of the droop approach took about 1 s to reach steady state behavior again, which is much higher while comparing to the approximately 2 cycle response time of the PBC and CBC methods. As discussed in [17], such time response of the PBC and CBC is fast, although it may vary depending on how fast the communication data link is configured for exchange of control data to occur during the coordination of the inverters. Although the classic droop control may present slower time response during load transients, as the one occurring between Intervals I and II, it presents the capability to share the transient power stress among PEIs. On the other hand, this does not occur to the PBC and CBC, which require the main grid or grid-forming converter at the PCC to support the transient power until the centralized strategy is able to readjust the operational setpoints for the distributed inverters.

It is interesting to note in Interval II that, although the behavior of the active power sharing is again similar among the three methods, following about $r_{PEIs} = 1.66$, the reactive power sharing provided by the classic droop method presented a significant change mostly on the operation of PEI_1. As the load changed, PEI_2 slightly adjusted its reactive power injection, while PEI_1 presented a large step in the reactive power processing. On the other hand, the PBC and CBC methods adjusted the sharing of reactive terms for both PEIs, still following the expected proportional ratio of about 1.66. The PEI's currents shown in Fig. 4(b) also highlight that, when droop control is employed, PEI_1 processes currents with higher amplitude than those from the PBC or CBC strategies.

Finally, in Interval III it can be seen another load step at 4 s when CB_L is switched on, allowing more power to be demanded by the loads. Once again, the active power sharing presents similar behavior for all three methods, apart from the slower response provided by the droop control, which also presents higher overshoot on the active power being processed by the inverters. The expected proportionality ratio of 1.66 occurs between the two PEIs for all strategies, in relation to the active power. In addition, similar to the previous case, the PBC and CBC adjust the sharing of reactive power also following the 1.66 ratio. Contrariwise, droop control leads both PEIs to share reactive power following a ratio of $r_{PEIs} = 5.99$, as seen in Table I. This demonstrates that PEI_1 processes much higher power than PEI_2 as a consequence of the relation of droop gains among PEIs, and due to the impact of having different line impedances among them. Note in Fig. 4(c) that greater amount of reactive power being processed by PEI_1 makes its current to be significantly phase-shifted in relation to PEI_2.

B. *Active and Reactive Power Sharing Upon Line Impedance Variation*

For this second scenario, a case in which the MG impedances change is considered to highlight the contrasts in operation between the classic droop-based methods and the PBC and CBC strategies. The same condition of Interval III is simulated for this case, having CB_{NL} switched off and CB_L switched on. At 6 s, considering the same previous control parameters for all strategies, the line impedance Z_3 is switched by a 2 times higher impedance (i.e., $Z_4 = 2xZ_3$). This case represents the interactive changes that may occur in LV MGs on which many active and passive elements are suddenly connected or disconnected from the grid, changing the equivalent impedance seen by the PEIs and by the upstream grid. The result of the active and reactive power sharing among the DGs is depicted in Fig. 5.

It can be noted from the results that the steady state behavior for the active power sharing reached a similar operation point for all the three strategies, although slight more power is processed by PEI_1 when droop control is implemented. Nonetheless, note that the droop method presented a significant and sudden overshoot, of about 20 %, in the active power processed by the PEIs, being positive for PEI_1 and negative for PEI_2. Additionally, the transient response of the droop-controlled inverters took much longer to accommodate than the previous cases when the load step was considered. It can be seen in Fig. 5 that the inverters took about 5 s to reach steady state, which is much higher than the previous scenario. Such results demonstrate how sensitive and dependent the classic droop control approach is to changes on the physical parameters of the

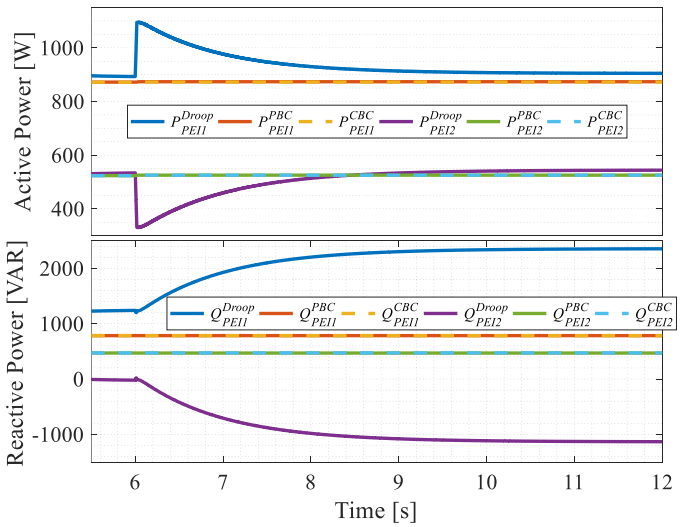

Fig. 5. Simulation results for the droop, PBC and CBC strategies sharing active and reactive power upon line impedance variation.

electrical circuit. Note that, even though active power is shared similarly, the reactive power processed by PEI_1 and PEI_2 presented, respectively, magnitudes approximately 3 and 2.4 times higher than the ones when the PBC and CBC methods were used.

To improve the time response capability of the system, the droop control gains and time constant of filters could be adjusted/optimized, as well as improvements in the classic droop strategy implemented could be made to overcome the limitations related to line impedances. Such alternatives have been extensively explored, such as in [4,7,15,26]. As can be seen by the active and reactive power in Fig. 5, the power oscillation caused by the droop method does not occur for neither the PBC nor the CBC methodologies. This happens because PEIs share power proportionality to their capabilities regardless of the grid's physical parameters, making the methods non-sensitive to variations on the electrical system, apart from those related to the PEIs power capabilities. The drawback of this feature of the PCB and CBC methods is that, by disregarding the features of line impedances over the MG, higher energy losses may occur depending on the node disposition of the PEIs and their power ratios.

V. Experimental Results

To reinforce the operational capabilities of the discussed centralized strategies, herein experimental results of the CBC approach are presented. Note that, as already discussed in Section IV, due to the similarity of operation between the PBC and CBC, experimental results are presented only for the latter strategy. The results are attained from a laboratory-scale prototype of a single-phase MG as shown in Fig. 2, only disregarding the linear load Z_{L2}. The setup comprises two full-bridge single-phase PEIs assembled using Semikron SKM 75GB128D IGBT modules, with 2.5 mH iron-core inductors as output filters. Linear and nonlinear loads are assembled replicating the ones used in Fig. 2 for the simulation results. The inverters are fed by a constant voltage source at their DC buses and the MG's PCC is coupled to the local utility, which imposes the 60 Hz, 127 V_{rms}, AC voltage to the circuit. The inverters use proportional resonant (PR) controllers designed as in [27], with control algorithms and the CBC strategy being implemented using a TMS320F28335 floating-point digital processor. The rated power values of PEIs are 5 and 3 kVA. As done in simulations, the CBC strategy is processed once in a fundamental cycle.

The results are shown in Fig. 7, being split into three stages. Firstly, in Fig. 7(a), the PEIs are disconnected and only the load draws current from the grid, as can be seen by the PCC current. Note that the currents are distorted due to the nonlinear load. At this moment, 489 W and 1268 VAR of respectively active and reactive

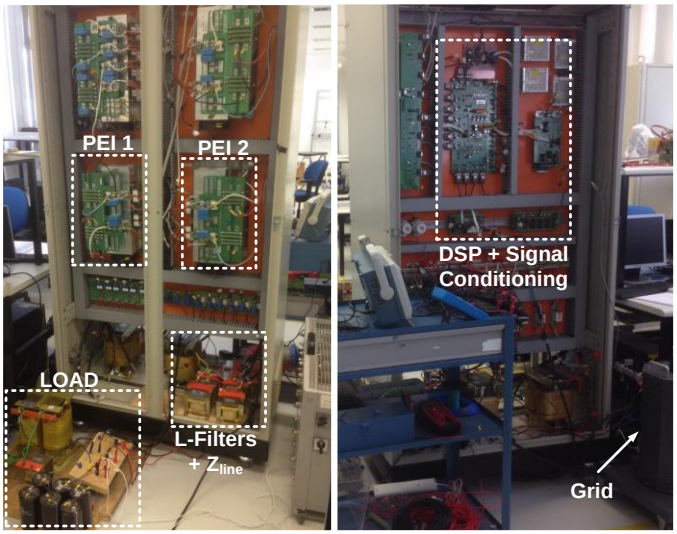

Fig. 6. Laboratory protype of the LV MG with two single-phase inverters.

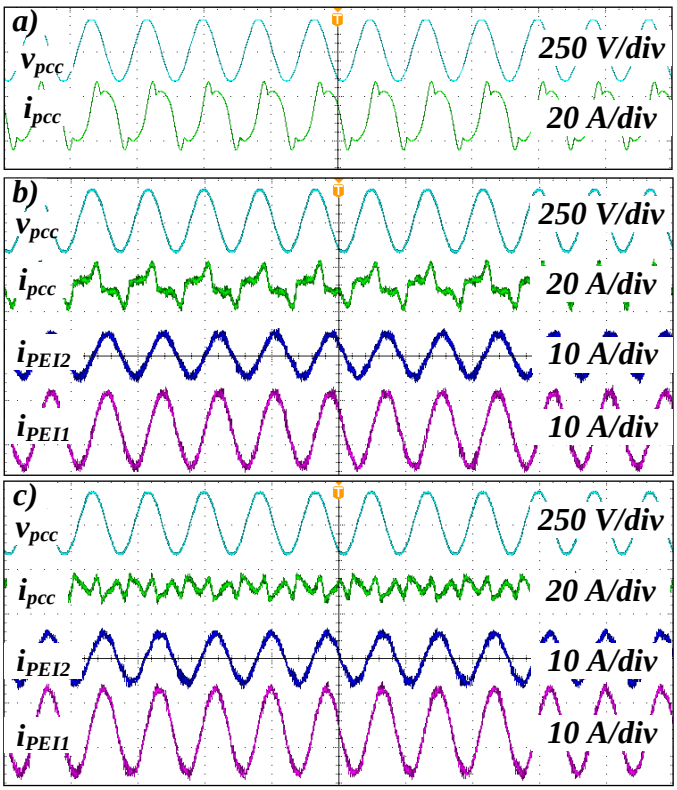

Fig. 7. Experimental results of the CBC strategy. a) Load currents; b) Sharing of reactive power; c) Sharing of active and reactive power.

power are circulating at the PCC. In Fig. 7(b), the second stage is shown with the steady state currents at the PCC and for PEI_1 and PEI_2. At this stage the CBC is set to share only reactive currents among the PEIs. Note that, as seen on the power curves in Fig. 3 and in the current waveforms of Fig. 4(a), the current of PEI_1 presents an amplitude approximately 1.6 times higher of that of PEI_2 due to the proportional sharing provided by the CBC. In

addition, since the inverters share the reactive power drawn by the load, the PCC waveform is now in-phase in relation to the grid voltage. The remaining PCC current is distorted because harmonic compensation is out of scope in this paper and it is not performed in Fig. 7.

Finally, the discussion on the performance of the centralized strategies are reiterated in regard to the capability to perform active and reactive power sharing among the inverters. Note in Fig. 7(c) that, upon setting the CBC to share the active and reactive currents, the PCC current is seen mainly being composed of harmonic terms. Moreover, the proportionality among the currents injected by the PEIs is maintained as in the previous case, being similar to Fig. 4(b). As aforementioned, different from the classic droop control method, the inverters share the same proportions of both active and reactive power, regardless of line impedances values. As a consequence, mostly harmonic currents flow at the PCC in Fig. 7(c).

VI. CONCLUSIONS

In this paper some considerations are raised in regard to how the PBC and CBC strategies, which are based on a master/slave architecture of coordinated control, can relate to the features of the well-known classic droop control approach. Focus is given to the ability to provide active and reactive power sharing in LV MGs. Firstly, for the PBC and CBC, it is highlighted a basic principle regarding their control topology, which is the dependence on having a grid-forming converter placed at the MG's PCC to support islanded operation. Contrariwise, droop-based methods are suitable for grid-connected and autonomous MGs, not requiring an interface converter at the MG's PCC. Additionally, even though VCM inverters may be accommodated by the PBC and CBC methods, their operation is only considered to follow a given power or current reference given for their output. Concerning the control topology of the classic droop method, grid-connected operation can be supported, although additional secondary control loops [4] are required to be implemented to provide power references for the inverters. Thus, the islanded operation mode was considered as basis for discussions in this paper, demonstrating that such method presents limitations concerning its reactive power sharing accuracy.

In regard to the steady state and transient behavior of the methods, it has been shown that the PBC and CBC present much faster response time, although being dependent on communication means. Moreover, these two approaches share active and reactive power among PEIs proportionally based on their power capabilities. On the other hand, even though classic droop control enables proportional active power sharing, it is not able to follow such concept for reactive power injection, which turns to be shared in different proportions among PEIs depending on how the droop gains are set, as well as depending on the features of the line impedances. Additionally, the impact of having variations in line impedances shows that the PBC and CBC does not need any previous knowledge about them, and that their dynamic behavior does not impact the active and reactive power sharing provided. Nevertheless, operation based on droop control is significantly affected by the line impedances.

Finally, experimental results were shown for the CBC strategy to reiterate its operational capabilities, which present similar features to the PBC strategy in relation to active and reactive power sharing. Future works aim at providing an experimental comparison among such three strategies, as well as exploring the particularities of the harmonic sharing provided by the CBC and droop-related approaches, such as the implementation of virtual impedances. Discussions related to the power dispatchability offered by the PBC and CBC strategies at the MG's PCC is also of interest for future studies, contrasting with the capabilities of droop-based methods.

ACKNOWLEDGMENT

The authors are grateful to the Sao Paulo Research Foundation (FAPESP) (Grants 2018/22172-1, 2017/24652-8, 2016/08645-9), and the Research Council of Norway (Grant f261735/H30).

REFERENCES

[1] M. Liserre, T. Sauter, J. Y. Hung, "Future Energy Systems: Integrating Renewable Energy Sources into the Smart Power Grid Through Industrial Electronics," *IEEE Ind. Electron. Mag.*, vol. 4, Mar. 2010.

[2] S. P. P. Davari, M. F. Firuzabad, F. Blaabjerg, "Standard Test Systems for Modern Power System Analysis: An Overview," *IEEE Ind. Electron. Mag.*, vol. 3, no 4, pp. 86-105, Dec. 2019.

[3] M. C. Renteria, D. S. Martin, J. M. Guerrero, "Microgrids Literature Review through a Layers Structure," *MDPI Energies*, vol. 12, Nov. 2019.

[4] J. M. Guerreo et al, "Hierarchical Control of Droop-Controlled AC and DC Microgrids—A General Approach Toward Standardization," *IEEE Trans. Ind. Electron.*, vol. 58, no 1, pp. 158-172, Jan. 2011.

[5] Z. Zeng, R. Zhao, H. Yang, "Coordinated control of multi-functional grid-tied inverters using conductance and susceptance limitation," *IET Power Electron.*, vol. 7, no 7, pp. 1821-1831, Jul. 2014.

[6] A. H. Yazdavar, M. A. Azzouz, E. F. El-Saadany, "A Novel Decentralized Control Scheme for Enhanced Nonlinear Load Sharing and Power Quality in Islanded Microgrids," *IEEE Trans. Smart Grid*, vol. 10, no. 1, pp. 29-39, Jan. 2019.

[7] F. Dorfler, J. W. S. Porco, F. Bullo, "Breaking the Hierarchy: Distributed Control and Economic Optimality in Microgrids," *IEEE Trans. Control Network Syst.*, vol. 3, no 3, pp. 241-253, Sep. 2016.

[8] Z. Cheng et al, "To Centralize or to Distribute: That Is the Question: A Comparison of Advanced Microgrid Management Systems," *IEEE Ind. Electron. Mag.*, vol. 12, no. 1, pp. 6-24, Mar. 2018.

[9] E. Harmon et al, "The Internet of Microgrids: A Cloud-Based Framework for Wide Area Networked Microgrids," *IEEE Trans. Ind. Inf.*, vol. 14, no 3, pp. 1262-1275, Mar. 2018.

[10] T. Caldognetto et al, "Power-Based Control of Low-Voltage Microgrids," *IEEE J. Emerg. Sel. Topics Power Electron.*, vol. 3, pp. 1056-1066, Dec. 2015.

[11] A. M. S. Alonso et al, "Considerations on Communication Infrastructures for Cooperative Operation of Smart Inverters," in *Proc. IEEE COBEP/SPEC*, Dec. 2019.

[12] Y. Han et al, "Review of active and reactive power sharing strategies in hierarchical controlled microgrids," *IEEE Trans. Power* Electron., vol. 32, pp. 2427–2451, Mar. 2017.

[13] T. D. C. Busarello et al, "Application of the Conservative Power Theory Current Decomposition in a Load Power-Sharing Strategy Among Distributed Energy Resources," *IEEE Trans. Ind. Appl.*, vol. 54, no 4, pp. 3771-3781, Mar. 2018.

[14] J. Rocabert et al, "Control of power converters in AC microgrids," *IEEE Trans. Power Electron*. vol. 47, no 11, Nov. 2012.

[15] G. Jin, L. Li, G. Li, Z. Wang, "Accurate proportional load sharing among paralleled inverters based on improved P-V droop coefficient," *Electr. Power Syst. Research*, vol 143, pp. 312-320, Feb. 2017.

[16] P. Sreekumar, V. Khadkikar, "Direct Control of the Inverter Impedance to Achieve Controllable Harmonic Sharing in the Islanded Microgrid," *IEEE Trans. Ind. Electron.*, vol. 64, no 1, pp. 827-837, Jan. 2017.

[17] A. M. S. Alonso et al, "A Selective Harmonic Compensation and Power Control Approach Exploiting Distributed Electronic Converters in Microgrids," *Int. J. Electr. Power Energy Syst.*, vol. 115, Sep. 2019.

[18] P. Tenti, D. Trombetti, E. Tedeschi, P. Mattavelli, "Compensation of Load Unbalance, Reactive Power and Harmonic Distortion by Cooperative Operation of Distributed Compensators," in *Proc. European Conf. Power. Electron. Appl.*, Sep. 2009.

[19] D. I. Brandao et al, "Centralized Control of Distributed Single-Phase Inverters Arbitrarily Connected to Three-Phase Four-Wire Microgrids," *IEEE Trans. Smart Grid*, vol. 8, no. 1, pp. 437–446, 2017.

[20] D. I. Brandao et al, "Coordinated Control of Distributed Three-and Single-phase Inverters Connected to Three-Phase Three-Wire Microgrids," *IEEE J. Emerg. Selec. Topics Power Electron.*, vol. PP, Jul. 2019.

[21] D. I. Brandao, L. S. de Araújo, T. Caldognetto, and J. A. Pomilio, "Coordinated control of three- and single-phase inverters coexisting in low-voltage microgrids," *Applied Energy*, vol. 228, Oct. 2018.

[22] G. Cavraro, T. Caldognetto, R. Carli, P. Tenti, "A Master/Slave Approach to Power Flow and Overvoltage Control in Low-Voltage Microgrids," *MDPI Energies*, pp. 1-22, Jul. 2019.

[23] A. M. S. Alonso et al, "Coordinated Control of Parallel Power Conditioners Synthesizing Resistive Loads in Single-Phase AC Microgrids," in *Proc. EPE ECCE Europe*, pp. 1-9, Sep. 2019.

[24] Q. Liu, T. Caldognetto, S. Buso, "Review and Comparison of Grid-Tied Inverter Controllers in Microgrids," *IEEE Trans. Power Electron.*, vol. PP, Dec. 2019.

[25] A. Micallef et al, "Reactive Power Sharing and Voltage Harmonic Distortion Compensation of Droop Controlled Single Phase Islanded Microgrids," *IEEE Trans. Smart Grid*, vol. 5, no 3, pp. 1149-1158, May 2014.

[26] R. Razi, H. Iman-Eini, M. Hamzeh, "An Impedance-Power Droop Method for Accurate Power Sharing in Islanded Resistive Microgrids," *IEEE J. Emerg. Sel. Topics Power Electron.*, vol. PP, Jul. 2019.

[27] S. Buso, P. Mattavelli, "Digital control in power electronics," Morgan & Claypool, 2nd Ed., 2015.